Icarus 287 (2017) 287–300

Contents lists available at ScienceDirect

Icarus

journal homepage: www.elsevier.com/locate/icarus

Present and past glaciation on Pluto

Alan D. Howard[a,*], Jeffrey M. Moore[b], Orkan M. Umurhan[b], Oliver L. White[b], Robert S. Anderson[c], William B. McKinnon[d], John R. Spencer[e], Paul M. Schenk[f], Ross A. Beyer[g,b], S. Alan Stern[e], Kimberly Ennico[e], Cathy B. Olkin[e], Harold A. Weaver[i], Leslie A. Young[b], the New Horizons Science Team

[a] Department of Environmental Sciences, University of Virginia, P.O. Box 400123, Charlottesville, VA 22904, USA
[b] National Aeronautics and Space Administration (NASA) Ames Research Center, Space Science Division, Moffett Field, CA 94035, USA
[c] Department of Geological Sciences, University of Colorado, Boulder, CO 80309, USA
[d] Department of Earth and Planetary Sciences, Washington University, St. Louis, MO 63130, USA
[e] Southwest Research Institute, Boulder, CO 80302, USA
[f] Lunar and Planetary Institute, Houston, TX 77058, USA
[g] The SETI Institute, Mountain View, CA 94043, USA
[i] The Johns Hopkins University Applied Physics Laboratory, Laurel, MD 20723, USA

ARTICLE INFO

Article history:
Received 6 March 2016
Revised 5 July 2016
Accepted 9 July 2016
Available online 16 July 2016

Keywords:
Pluto, surface
Ices
Geological processes

ABSTRACT

Modern N_2 ice glaciers flow from highlands to the east of the $750 \times 1400\ km^2$ lowland of Sputnik Planum [***SP***] and merge with the ices of similar composition on ***SP***. We explore the possibility that glaciation may be fed by N_2 sublimation from ***SP*** followed by redeposition on the highlands. The uplands to the northeast, north, and west of ***SP*** have been erosionally sculpted into a variety of dissected terrains that feature linear depressions (valleys), locally in dendritic networks. We interpret these dissected terrains to have been carved by N_2 glaciers formerly covering the uplands. Depositional glacial landforms (moraines, eskers, outwash) have not been identified, however. N_2 glaciation would have a different erosional manifestation because the substrate (porous water ice and CH_4-rich mantles) probably has lower density than N_2, and also because of the lack of freeze-thaw weathering. If sufficiently thick (1–4 km), N_2 glaciers might have experienced basal melting. Past flow of N_2 glaciers from the highlands into ***SP*** may have detached and transported the prominent mountainous water ice mountains along the western border of ***SP***.

1. Introduction

Pluto has experienced a rich geologic history involving surficial processes driven by volatile exchanges and transport – which continue to the geologically recent. The New Horizons spacecraft has imaged the anti-Charon side of Pluto with resolutions ranging from 497 to 93 m per pixel (Fig. 1). The equatorial region is dominated by the flat plain of Sputnik Planum[1] [***SP***], an expanse of about $750 \times 1400\ km^2$ dominated by N_2 and CO ices that are probably involved in convective overturning of 10-40 km diameter cells (McKinnon et al., 2016; Trowbridge et al., 2016), sporting a surface densely pockmarked by sublimation pits characteristically a few hundred meters across (Stern et al., 2015a; Moore et al., 2016). A total absence of resolvable impact craters implies that the surface age of ***SP*** is likely no greater than 10 Ma (Moore et al., 2016). ***SP*** is surrounded by uplands typically 3-4 km above the plains of ***SP***. On the west, north, and northeast sides, these uplands contain numerous impact basins, indicating that the uplands date to early Solar System history (Moore et al., 2016). These uplands have been modified by younger mantles and volatile-related geomorphic processes, including features interpreted here to have been formed by former glacial activity (Moore et al., 2016), and are likely underlain by a water ice crust (or basement) indicated by its high relief and local spectral identification (Stern et al., 2015a). Along the western margin of ***SP*** chains of mountainous water ice blocks up to 30 km across and up to 3.5 km high are separated 40–80 km from the uplands to the west by SP ices and low-relief fields of smaller blocks. Rough-textured, pitted uplands with high albedo extend about 550 km eastward along 750 km of the eastern margin of SP, forming the eastern half of the high-albedo feature called Tombaugh Regio, which also includes ***SP***. The western margin of this upland is the source region for recently-active glaciers discussed below.

* Corresponding author.
E-mail address: ah6p@virginia.edu (A.D. Howard).
[1] All feature names on Pluto are informal.

http://dx.doi.org/10.1016/j.icarus.2016.07.006
0019-1035/

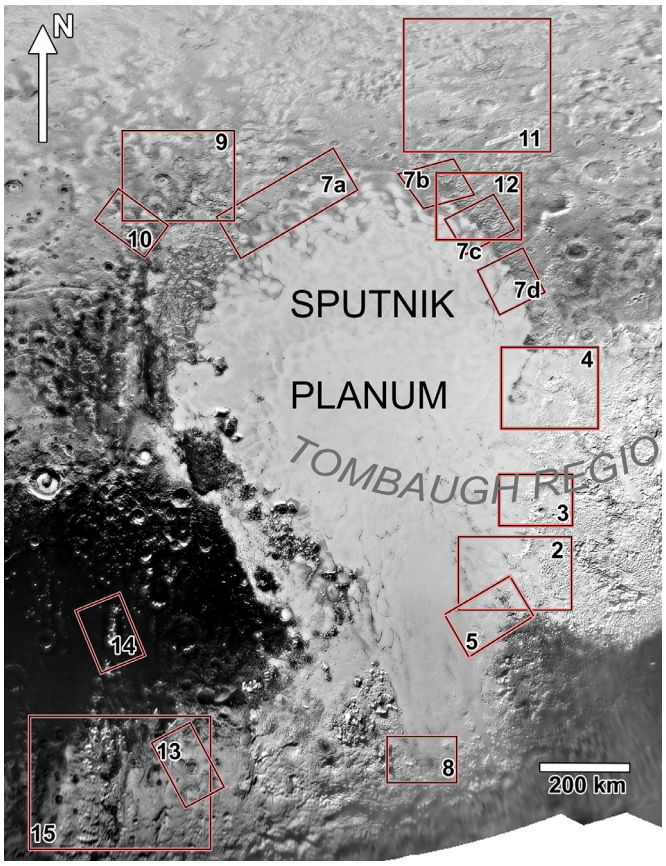

Fig. 1. Overview of the glacial region on Pluto. Numbered boxes refer to figures. Longitude range 32-213°W, latitude range 32°S to 68°N. Image base is MVIC PEMV_01_P_MPAN1 with lower resolution global coverage at southern latitudes. Feature names on Pluto are informal."Sputnik Planum" refers to the low relief bright surface extending south to the location of Fig. 8. "Tombaugh Regio" includes Sputnik Planum and the high-albedo uplands to the east and southwest.

1.1. Properties of relevant materials and surface temperatures

The landforms and processes discussed here involve several ices – N_2, CO, CH_4, H_2O, and possibly liquid N_2. We summarize their densities and rheological properties as a basis for the discussion below.

Surface Temperature: At present the surface temperature of Pluto averages about 38 K (Stern et al., 2015a), although occultation data from New Horizon's Radio Experiment (REX) indicates surface temperature of 45 K (Gladstone et al., 2016). The temperature of pure nitrogen ice surfaces under direct solar illumination is largely controlled by sublimation cooling to about 35 K (Lellouch et al., 2000), suggesting that the N_2 on the surface may not be pure. Temperatures over other, non-N_2 surfaces can reach 60 K, particularly near the subsolar latitude (Lellough et al., 2011; Hansen et al., 2016; Levrat et al., 2016). The distribution of surface temperature is strongly influenced by seasons and obliquity variations (Earle et al., 2016). The interaction of its 6.4 day rotation period, its 248 year orbital period, an inclined and elliptical orbit, and a 2.8 Myr obliquity cycle produce a complicated temporal pattern of insolation and associated climatic zonation. During the last ~1.3 Myrs the high northern latitudes have received the greatest integrated insolation (Earle and Binzel, 2015).

Densities of ices at 45 K ($gm\,cm^{-3}$) are: N_2 0.98; H_2O 0.94; CH_4 ~0.4, CO 1.01 (Scott, 1966; Fracassi et al., 1986; Petrenko and Whitworth, 1999; Satorre et al., 2008). Liquid N_2 at 77 K has a density of 0.81. Water ice comprises the crustal bedrock and may be porous, and hence lighter than cited above due to impact fracturing, possibly down to $0.8\,gm\,cm^{-3}$ (Grundy et al., 2016; Moore et al., 2016). CO has been detected on ***SP*** in uncertain quantities, however its density and rheology are close to those of N_2 (Fukushima et al., 1977; Moore et al., 2016). In this paper when N_2 ice and its properties are discussed, an unknown amount of CO ice may be admixed.

Rheology: At the present surface atmospheric pressure of Pluto, N_2 and CH_4 are well below their triple point so that a liquid phase is unstable. Stern et al. (2016) suggest under certain obliquity conditions surface temperatures might rise sufficiently to result in N_2 melting. Water ice is essentially rigid over geologic time scales at Pluto's surface temperature and can support several km of relief (Stern et al., 2015a). N_2 ice with some admixture of CO and CH_4 (Philippe et al., 2016; Schmitt et al., 2016) forms the dominant solid on ***SP*** and is involved in convective overturning and the glaciation discussed below (Stern et al., 2015a; Moore et al., 2016). It is useful to compare the strain rates for H_2O ice at typical terrestrial temperatures and shear stresses for terrestrial glaciation (263 K and 100 kPa) with N_2 ice at representative Pluto temperature and lower gravitational shear stress (45 K and 10 kPa). For the terrestrial case deformation would be by grain boundary sliding with strain rates in the range of 3×10^{-10} to $8\times10^{-10}\,s^{-1}$ for 1 mm grains (Paterson, 1994; Petrenko and Whitworth, 1999; Durham and Stern, 2001; Goldsby and Kohlstedt, 2001). Few measurements have been made of rheology of N_2 ice. For the specified conditions for Pluto experiments by Yamashita et al. (2010) suggest a strain rate of $3.2\times10^{-7}\,s^{-1}$, three orders of magnitude more deformable than terrestrial glaciers. The convective overturning of ***SP*** ice and its young surface age (<10 Ma) (Stern et al., 2015a; Moore et al., 2016) are consistent with this high mobility. The rheology of ices, however, varies strongly with temperature, grain size, chemical and particulate content, and strain history, and measurement of rheological properties are made at strain rates much higher than at planetary conditions. CH_4 ice spectral signatures are strong on high relief terrain on Pluto's highlands (Grundy et al., 2016), and admixtures of CH_4 and water ice may dominate on steeper slopes on the highlands. At 45 K and 19 kPa shear stress measurements by Yamashita et al. (2010) indicate a strain rate of $1.7\times10^{-9}\,s^{-1}$ Earlier measurements and calculations of CH_4 by Eluszkiewicz and Stevenson (1990) suggest much lower deformability. The rheology of all ices is strongly dependent on temperature and grain size. N_2 ice flow is also strongly affected by climatic evolution (Earle et al., 2016). The deep-seated convective cells of the nitrogen-rich central regions of SP are discussed in McKinnon et al. (2016) and Trowbridge et al. (2016), where the effect of the geothermal gradient on N_2 ice rheology and convection is discussed. Preliminary quantitative modeling of nitrogen glacial flow is presented in Moore et al. (2016, SOM) and Umurhan et al. (2016).

In summary, at Pluto water ice can be considered to be rigid, methane deforms only over geologic timescales, but N_2 flows much more readily than terrestrial water ice despite the lower gravity. Because of the inclined, elliptical orbit of Pluto, insolation patterns shift dramatically over ~2.8 Myr cycles, so that the spatial patterns of volatile distribution may shift dramatically.

2. Features of the eastern margin of Sputnik Planum

Nearly flat expanses tens of km across of nitrogen-rich ices lie 2–3 km above the floor of ***SP*** and are connected through several trough-like valleys to the surface of ***SP*** (e.g., Fig. 2).[2] Fig. S1 shows

[2] Latitude and longitude on Pluto are defined according to the right hand rule. Pluto's North pole points in the direction of the angular momentum vector and longitudes increase to the East (sub-solar longitudes thus decrease in time). Pluto's prime meridian is the sub-Charon longitude. Pluto's pole is defined

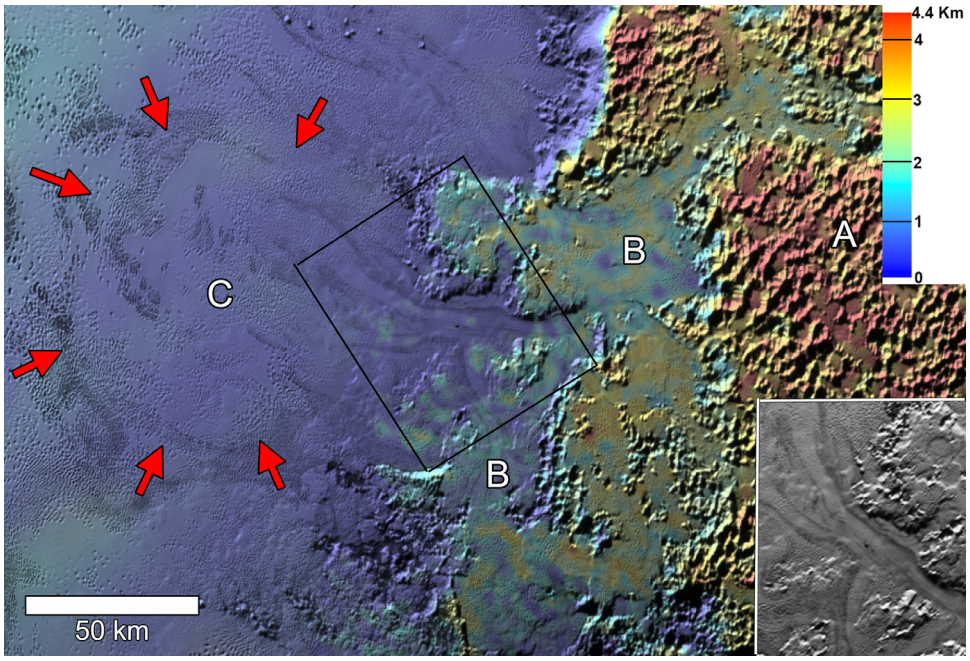

Fig. 2. Nitrogen ice-related features on the boundary between Sputnik Planum (**SP**) and highlands to the east. "A" indicates pitted uplands with a strong methane ice spectral signature and probable admixture of water ice. Points labeled "B" denote ice flats at several levels up to 1.5 km above **SP**, which constitutes the western half of this image. "C" is ices on **SP** that are bordered by dark banding. Both **SP** and the icy flats have prominent signatures of N_2 ice. The inset covers the area shown in the black box. This region highlights dark bands converging from the highland ice flats through a ~6 km wide channel connecting the ice flats "B" to **SP** and diverging into **SP** within region "C". These dark bands are interpreted to constitute flow bands similar to medial moraines on terrestrial glaciers, such that N_2-rich ices from "B" flow out to **SP** and pond in region "C" bounded by the red arrows. Image and inset are MVIC high phase angle image (340 m/pixel). PEMV_01_P_MVIC_LORRI_CA. See Fig. S1 for a stereo anaglyph image of this region. North is up. (For interpretation of the references to color in this figure legend, the reader is referred to the web version of this article).

the same region in an anaglyph stereo image. Such connected flats extend up to 100 km beyond the eastern margin of SP. Other, but isolated, N_2-rich plains extend more than 300 km to the east as isolated patches on the high-albedo uplands of Tombaugh Regio. The N_2-rich flats are surrounded and generally enclosed by rough, pitted uplands with a strong methane spectral signature. The 2–5 km wide troughs connecting the icy flats to ***SP*** are floored with N_2-rich ices and slope about 2%. Because of the smooth surface of the N_2 ice surfaces at the resolution of stereo imaging (~500 m) DEM generation using automated tie point matching produces apparent waviness on the N_2 flats (Fig. 2); stereo anaglyphs (Fig. S1) demonstrate that these are artifacts. Topographic gradients over a few hundred km are, however, likely accurate within a factor of two. The stereo anaglyphs reveal that the upland flats systematically decrease in elevation where they border the troughs. High phase angle imaging by the MVIC scanning imager (340 m/pixel) reveals dark bands on the icy surfaces up to 1.5 km wide. These bands start on the N_2 upland flats, converge within the throats of the connecting valleys, and expand onto ***SP*** (Figs. 2, S1).

Similar connections through narrow valleys between upland N_2-rich flats and ***SP*** occur along the 700 km boundary between ***SP*** and the high-albedo, pitted uplands to the east (e.g. Figs. 3, 4, S2, S3). In several locations the connecting valleys display short, steep drops but appear to be floored by N_2-rich ices. As shown in Fig. 3, at the lower end of the narrow valley connecting upland N_2 flats to SP, the valley expands into a fan-shaped form sloping toward the interior of ***SP***.

Within 100 to 200 km of its eastern edge, the floor of ***SP*** has morphology that is distinct from the cellular pattern characteristic of central ***SP*** (Fig. 1). At several locations, particularly at and near the region shown in Fig. 2, dark bands a few km wide extend toward the interior of ***SP*** from its eastern margin, including the banding spreading eastward from the valley shown in Fig. 2. In the region detailed in Fig. 2 dark bands enclose a 100-km wide region in which the dark bands radiate from the valley (red arrows in Fig. 2). North of this region the dark bands include, or are replaced by, steep sided mounds and clusters of mounds 1–5 km in diameter that rise up to several hundred meters above the ***SP*** ice

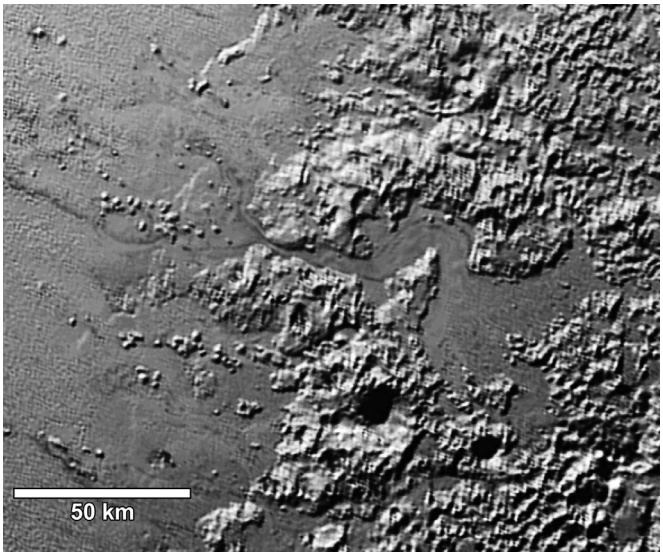

Fig 3. Glacial flow through a 2 km-wide trough into **SP**. Note flow lines and fan-like deposit of ice on **SP** just beyond the trough termination. Blocks of about 1 km diameter protruding above **SP** ices may be broken-off parts of the pitted uplands ice-rafted through the trough onto **SP**. North to top. Part of PEMV_01_P_LORRI_CA image at 340 m/pixel. See Fig. S2 for a stereo anaglyph figure of this region. North is up.

as RA = 132.993°, Dec=-6.163° w = 302.695° wdot=56.3625225°/day (Archinal et al., 2011a, b).

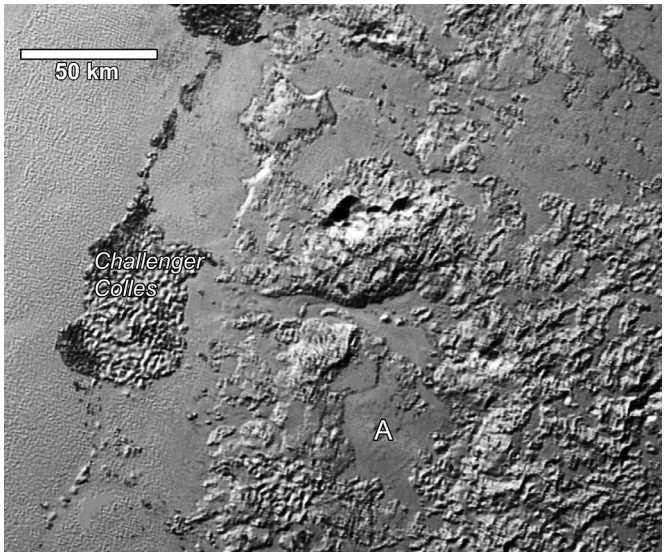

Fig. 4. Glacial flow from N_2-rich upland plains through a 2.5–6 km wide trough onto SP. The line and large collection of blocks on **SP** (Challenger Colles) are interpreted to be detached pitted uplands material that has been ice-rafted up to 40 km into SP. The icy flats at the upper right are separated from SP by scarps and may not be actively flowing onto **SP** at present. Parts of the icy flat at "A" are likewise largely isolated from the trough and may not be presently active. Part of PEMV_01_P_MVIC_LORRI_CA image at 340 m/pixel. See Fig. S3 for a stereo anaglyph version of this region. North is up

surface. The largest of these clusters of blocks is the 30×60 km^2 Challenger Colles (Figs. 4 and S3). Most of these dark bands and linear collections of blocks enclose lobe-like expanses extending from the margin of ***SP*** toward its interior. Similar ~1 km blocks are embedded within the upland N_2 flats and within the narrow troughs connecting the upland flats to ***SP*** (Figs. 3, 4, S2, S3).

Both the N_2-rich surface of ***SP*** and the upland flats display nearly ubiquitous sparse to dense pitting ranging in size from 200 m to 2 km across. Some of these are elongated into dark-floored grooves up to 10 km long (Fig 5). This pitting is difficult to resolve in 340 m/pixel imaging (Figs. 2–4) but becomes prominent in 93–120 m/pixel imaging (Fig. 5). Some of the elongated pits in Fig 5 are concentrated within, and extend along, the dark bands on ***SP*** discussed above.

In places the N_2-rich upland ices display a wavy topographic texture with 2–5 km spacing. This texture appears on steeper regional slopes and appears to consist of relatively flat treads and steeper downslope-facing risers that are often lobate in planform (Fig. 2). Some of these undulations occur on the surface of the ice within the troughs connecting the upland flats to ***SP*** (Figs. 2, S1).

2.1. Interpretation: modern glaciers

We interpret the landform assemblage discussed above to result from geologically modern glaciation routing N_2-rich ices from the uplands onto the floor of ***SP***, accompanied or followed by minor sublimation pitting and interaction with deeper-seated convection (McKinnon et al., 2016; Trowbridge et al., 2016). This interpretation is supported by several lines of evidence:

1. The upland N_2-rich surfaces slope in the inferred direction of flow and the steepest slopes occur where the flow would funnel through the trough-like valleys.
2. The dark banding observed on the N_2 ices aligns with the topographic slope. We suggest these are analogous to medial moraines or crevasse zones on terrestrial glaciers. These inferred flow lines diverge when emerging onto the ***SP*** lowlands (Fig. 2).
3. Subtle banding, pitting and, in some cases lines of knobs define the apparent limits of flows emerging onto ***SP***.
4. Fan-like forms occur at some locations where ice-filled troughs emerge onto ***SP*** (Fig. 3).
5. The low viscosity of N_2 ice implies appreciable flow rates would occur on the observed topographic slopes (up to a few degrees) unless the N_2 ice is very thin (Umurhan et al., 2016).

We suggest that the km-scale blocks on ***SP*** that occur as isolated blocks, stringers, and larger collections were ice-rafted from the uplands onto ***SP*** (Moore et al., 2016; McKinnon et al., 2016). Some such blocks occur within the troughs as well as on the upland flats. Their texture and scale is similar to parts of the pitted terrain enclosing the upland flats. This interpretation implies that these blocks are less dense than N_2 ice; spectral imaging shows that the larger accumulations of these blocks are methane rich and N_2-poor (Grundy et al., 2016), and may contain porous water ice as well. Both methane and water ices are less dense than N_2 ice.

Fig. 6 shows our interpretation of the glacial system that extends along the 700 km eastern margin of ***SP***. The extent of upland icy flats that have recently contributed flows into ***SP*** is shown by the purple line. The blue line shows our interpretation of the extent of geologically recent flows onto ***SP*** from the east, enclosing lobate features delineated by dark bands (e.g., red arrows in Fig. 2), lines of blocks, and locally by the km-scale sublimation troughs whose orientation may be controlled by textures in the underlying ice due to layering, foliation, or fracturing. The extent of N_2 ices involved in recent glaciation is shaded red. The brown line shows a possible earlier margin of N_2 ice flows as suggested by isolated groups of km-scale blocks. This outer border may correspond to a former larger ice sheet, or may have resulted from net basin-ward displacement of the boundary resulting from advection of new ice into the eastern margin of ***SP***. Between the blue and brown lines the block distribution appears to have been affected by cellular convection within the N_2 ice, rafting the blocks to the downwelling cell edges, where they collect (Moore et al., 2016, SOM), consistent with this terrain being older. If the terrain between the brown and black lines in Fig. 6 corresponds to a formerly greater glacial ice extent, causes might include climate change, diminished N_2 ice inventories, and evolution of upland morphology, such as by glacial scour (e.g., Anderson et al., 2012). The lack of cellular morphology in recent ice accumulations on SP may be due to shallow ice or lack of elapsed time for convection to become established.

2.2. Age, ice sourcing, and evolution of glaciation

There are no unambiguous craters on the N_2-rich surfaces on the uplands east of ***SP***, within the troughs connecting them to ***SP***, or on ***SP*** itself. This suggests that the surface age is less than 10 Ma (Moore et al., 2016) as the low viscosity of N_2 ice can eradicate craters over that time period (Stern et al., 2015b). The glacial system and most of the landforms we witness have likely evolved over a much longer period. The glacial systems shown in Figs. 2–4 are likely active at present. Flow rates are uncertain, however, due to lack of knowledge about ice thickness and the incomplete characterization of N_2 rheology.

The very young age of the active glacial systems and the high potential for rapid flow of N_2 ices due to its low viscosity poses a puzzle when faced with the antiquity of Pluto. We acknowledge several solutions to this puzzle: (i) some recent event may have placed or uncovered large reservoirs of N_2 ice on the uplands, (ii) a long-term gradual evolution has occurred, or (iii) a glacial cycle is involved in which N_2 ices are recycled onto the uplands to the east of ***SP***, analogous to the hydrological cycle feeding terrestrial glaciers. The high albedo of the Tombaugh Regio uplands east of

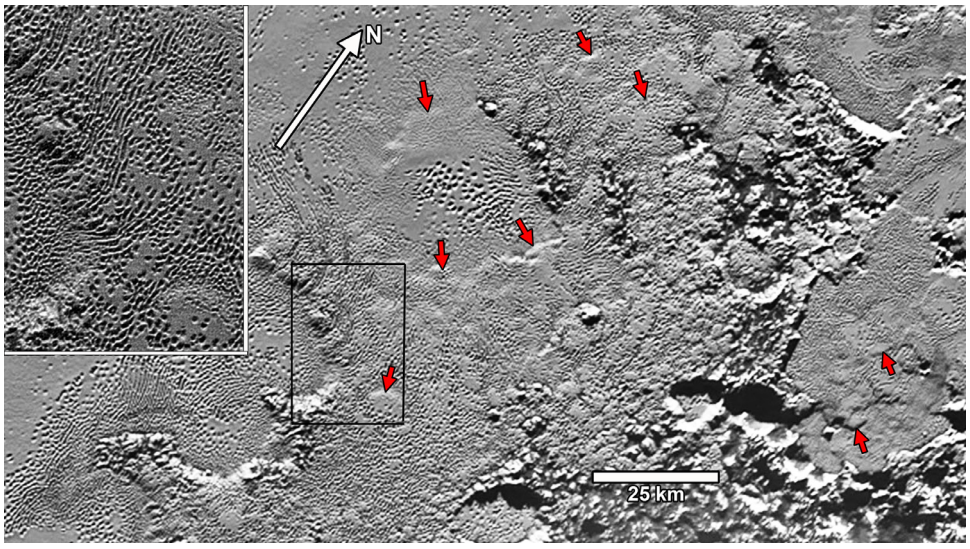

Fig. 5. Smaller geomorphic features of N_2-rich ices on **SP** and on upland plains. Sublimation pits typically 100-300 meters in diameter cover most of the icy surfaces within this image (see high-resolution inset of area indicated by black box). Red arrows point to step-like lobate structures typically 2–5 km in wavelength occurring locally on steeper ice slopes. These could be expressions of the underlying bedrock or possibly from flow instability. LORRI 93 m/pixel image mosaic PELR_P_MVIC_LORRI_CA. (For interpretation of the references to color in this figure legend, the reader is referred to the web version of this article).

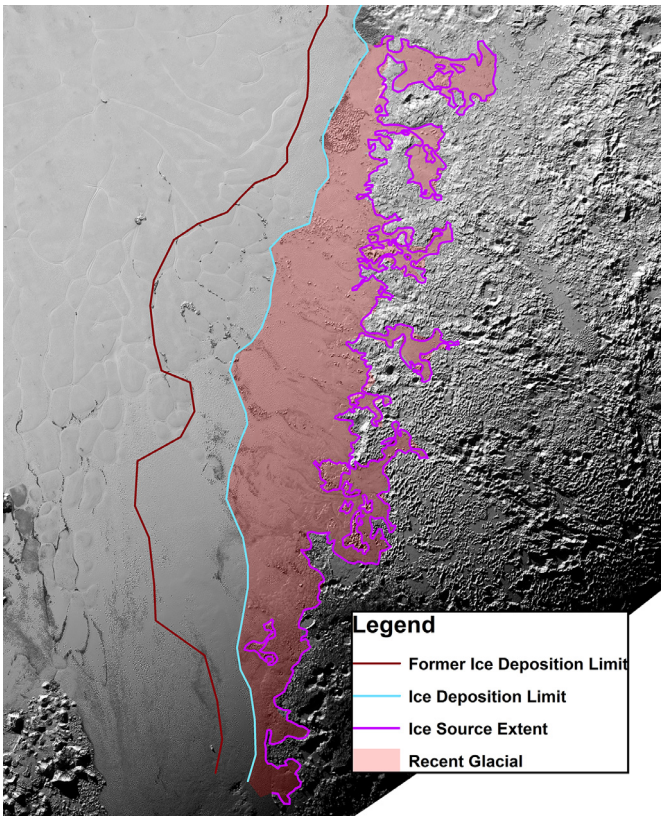

Fig. 6. Map of modern glacial features on the east side of **SP** and contiguous uplands. Violet line shows upland extent of ices inferred to be contributing or to have geologically recently contributed N_2-rich ice flowing onto **SP**. Blue line shows inferred extent of relatively recent flows onto **SP**. Brown line shows possible former extent of ice flow in the past (but still relatively geologically recent). Green "#" symbols mark short steep sections in troughs connecting upland flats to **SP**. These may be "throttle" points restricting flow rates with shallower mobile ice flowing over resistant stubstrate. Base map is MVIC PEMV_01_P_MPAN1 image. North is up. (For interpretation of the references to color in this figure legend, the reader is referred to the web version of this article).

SP is suggestive of recent ice deposition (Fig. 1). We suggest that these ices are sourced by sublimation of ice from the surface of ***SP*** (as suggested by the sublimation pitting) and are partially redeposited on the eastern uplands due to atmospheric circulation and recondensation. Such a system could potentially result in a steady glacial cycle. There are difficulties with this scenario, however. The uplands are nearly uniformly bright, and both the icy flats and the pitted terrain display a strong methane signature. N_2 ices, however, seem to be limited to the flats. The N_2 ices do not seem to derive from flow sourced from the pitted uplands; no consistent relationship between the size of N_2 ice flats and potential upland drainage areas exists. This suggests preferential deposition of N_2 ices on existing N_2-rich ice flats, whereas more methane-rich ices are deposited on the pitted terrain. Spectral analysis of ices from the LEISA spectrometer indicate that surface ices tend to be either nearly pure N_2 with less than 4% CH_4, or nearly pure CH_4, suggesting that intermediate compositions are unstable (Philippe et al., 2016; Schmitt et al., 2016).

A longer-term evolution may have taken place such that the uplands east of ***SP*** were once covered with more extensive N_2-rich ice deposits, and these have gradually been depleted, partly via sublimation and possible ultimate loss to space, and partly by glacial flow back into ***SP***; in this scenario, we may be witnessing the end-stages of this system. The scattered occurrence of N_2-rich ice flats several hundred km east as inliers within the pitted uplands might be consistent with this scenario. A decline in glacial activity through time may be indicated by the occurrence of sets of km-scale blocks on ***SP*** suggestive of greater past glacial flow that has either diminished or ceased at present. For example, in Fig. 4 the line of blocks on ***SP*** paralleling the uplands but separated from them by 30 km suggests former ice flow, but the upland icy flats at the upper center are separated from ***SP*** by a steep scarp with little evidence of current ice flow. Similarly, much of the N_2-rich icy flat at right center is isolated by a scarp from the ices flowing through the trough to ***SP***. These isolated uplands, however, display possible terraces suggestive of a former higher ice level. The large collection of blocks (Challenger Colles) at the mouth of the current trough would likely have required vigorous flow from the uplands, which does not appear to be happening at present.

A cycle of N_2 ice accumulation, strong glacial flow, followed by waning activity might be favored by the strong astronomical forcing of Pluto's solar illumination, with the longest cyclical forcing of 3 Ma (Earle and Binzel, 2015). The region with glacial flows is centered at about 10°N, which lies in the permanent tropics (where the Sun reaches the overhead point at least once per orbit) and mostly in the permanent diurnal zone, which never experiences arctic seasons (Binzel et al., 2016). Nonetheless, the high obliquity induces volatile migration which may cause atmospheric pressure excursions several orders of magnitude greater than the present value, perhaps allowing liquid N_2 or CO on the surface (Stern et al. (2016)).

All of the evolutionary and cyclical explanations for the modern glaciation on Pluto appear to involve tens of millions of years at most, which is difficult to reconcile with the ~4 Ga age of Pluto as indicated by its cratering record unless glaciation has been nearly continuous throughout its history or alternatively related to episodic N_2 resupply due to endogenic processes.

2.3. Flow and topography on Sputnik Planum

Stern et al. (2015a) noted albedo banding in the ***SP*** surface suggestive of modern flow of ices along its northern margin. The inferred sense of motion is from the center of SP toward the edges. The banding pattern is interpreted to correspond to advection and distortion of former convection cell boundaries. Anaglyph stereo imaging (Fig. 7) indicates that these features are associated with locally steep topographic gradients toward the edge of ***SP*** and, in several cases, topographic lows bordering ***SP***. At locations 2 and 8 in Fig. 7, a strong convergence of banding suggests, but does not prove, that appreciable localized flow has occurred toward the edge of ***SP***, implying localized mass loss of ice, perhaps to the subsurface.

At the southern margin of ***SP***, the ice surface topography plunges sharply to the south, dropping about 1–2 km in 50 km, a 2–4% slope (Fig. 8). This elevation decline is toward a deep depression in the bedrock at the edge of ***SP***. Near the southern edge of the ***SP*** ices, the surface exhibits a step-like, lobate topography similar to that observed on the glacial features observed in Fig. 5. About 130 km to the east a similar but narrower finger of N_2-rich ices slopes southward to the ***SP*** boundary. Given the low viscosity of N_2 ices, this steep gradient implies high southward flow rates into the depression, especially if the ***SP*** ices are thick.

With the exception of the inferred inflow of glaciers along the eastern margin of ***SP*** and the outward flow discussed here, most of the boundary between ***SP*** and the surrounding uplands appears to imply no net ice flow either toward or away from the boundary, because the ice surface is nearly level at the contact and there are not banding features on the ice suggestive of flow.

2.4. Recent history of Sputnik Planum

The young effective surface age of ***SP*** based on the lack of impact craters (Moore et al., 2016) likewise implies that the flow features on ***SP*** discussed above are also young; because of their larger scale, however, they may have a somewhat older effective age. Here we examine the implications of the inferred ice flow toward the margins of ***SP*** at its northern and southern edges by examining several possible scenarios:

(1) The flows toward the boundaries occur because net sublimation increases from the center of SP toward the northern and southern edges of ***SP***. The center of ***SP*** is at about 26°N, its northern boundary is at about 45°N and the southern boundary with the inferred outward flow is at about 22°S. During the past 2.5 Ma the average solar energy flux increases sharply towards northern latitudes (Earle and Binzel, 2015). Higher sublimation rates might therefore incite compensatory northward flow to replace ices lost to sublimation. During the decades after its discovery in 1930, average insolation was observed to increase towards the South Pole, potentially explaining the southward flow. However, it seems unlikely that this few decades of relatively high radiation loading could account for the strong observed topographic gradient.
(2) Northward and southward ***SP*** ice flow is a response to influx of N_2-rich ices from the modern glaciation on ***SP***'s eastern equatorial region. This could be consistent with a steady-state scenario in which sublimation of ice from ***SP***, particularly along its northern margin is balanced by return flow from N_2 ices deposited on its eastern margin and returned by glacial flow.
(3) The northward and southward flows are due to a volume increase of ***SP*** ices unrelated to glacial influx, because of unspecified geophysical processes.
(4) Sputnik Planum is losing N_2-rich ices to the subsurface at its northern and southern boundaries. The apparent convergence of flow lines toward depressions along the ***SP*** boundaries could be consistent with this scenario. If this is happening, it might imply subsurface migration of N_2, perhaps at depths of a few km where N_2 might be liquid.

No compelling evidence favors any of these scenarios at present. None of them are necessarily exclusive, nor do they exclude other scenarios.

3. Upland geomorphology

The ancient uplands surrounding ***SP*** to the west, north, and northeast feature a variety of erosional morphologies, primarily expressed as linear depressions, broadly described here as valleys without genetic implication. Several intergrading morphologies characterize portions of the uplands, described separately below. In addition, widespread low, parallel ridges termed here "washboard terrain" emboss portions of the uplands as described by Moore et al. (2016).

3.1. Fluted terrain

Steeper slopes on much of the northwestern rim of ***SP*** are sculpted by ridge and trough sets, such that troughs are spaced at about 2–3 km intervals (Figs. 9 and 10). These ridges and troughs are oriented downgradient on hillslopes that characteristically have gradients of about 20° and slope lengths of 2–5 km, measured horizontally. Vertical relief from summits to trough termination at basin floors can exceed 2 km. We informally term such ridge and trough sets "fluted terrain". In places hills about 20 km across are entirely dissected by flutes radiating in all directions from the hill summits. Interior crater walls are commonly also fluted. The ridges and troughs extend nearly to divides and generally terminate at crater floors or at relatively flat-floored depressions. In places these depressions are elongated into valleys that can exceed 100 km in length and be 10 or more kilometers wide. The downslope terminations of troughs characteristically lack identifiable deposits (e.g. fans or debris aprons). In some cases it appears that slopes dissected by fluting expose two layers, an upper, light-toned material lacking deep flutes underlain by a darker, deeply dissected unit (Figs. 9 and 10). Individual troughs rarely branch, and instead generally parallel each other. In a few locations, however, troughs appear to merge downslope at acute included angles, suggesting weak dendritic structure.

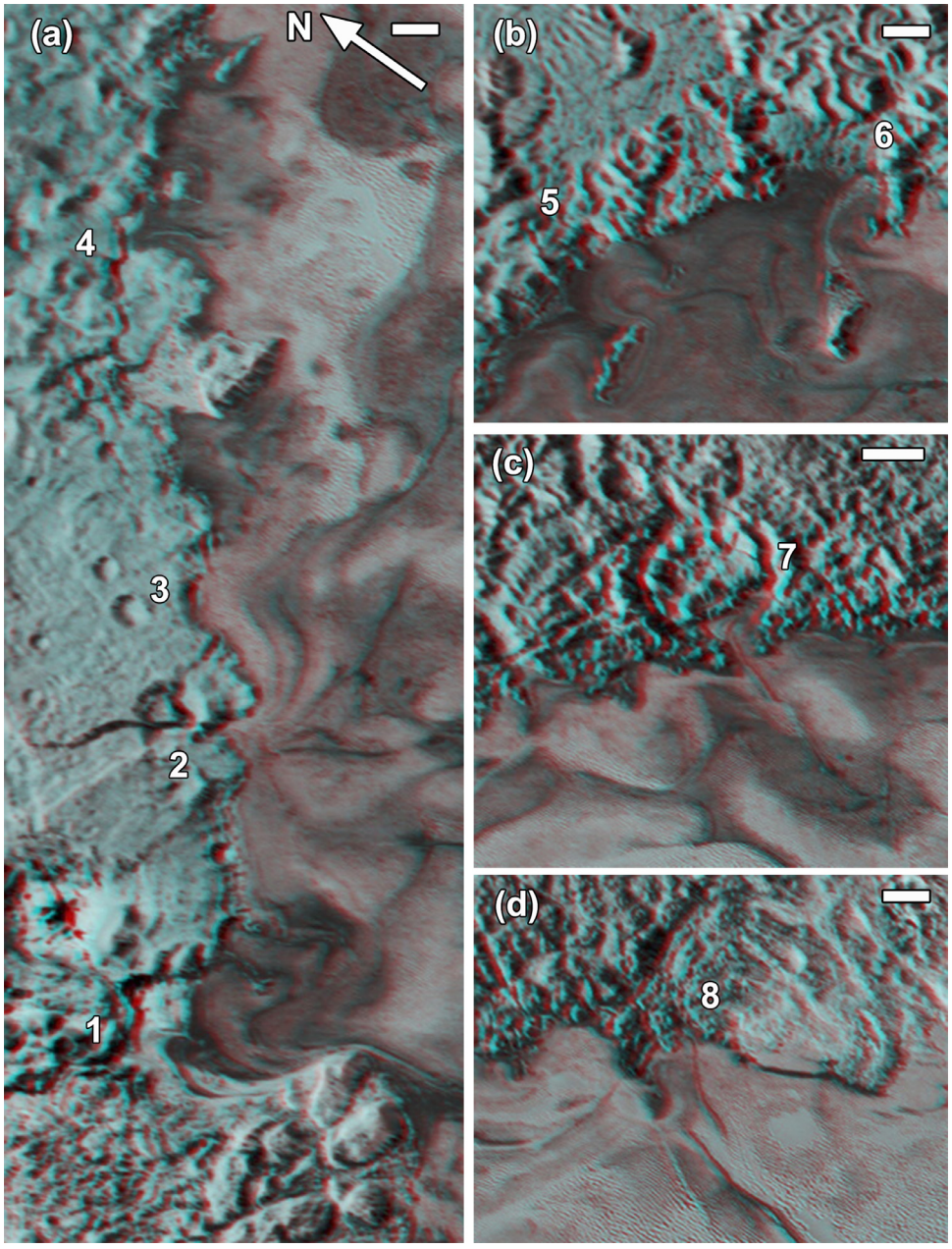

Fig. 7. Stereo anaglyph images of locations on northern boundary of **SP**, showing probable flows from interior of **SP** toward low points in the contiguous uplands. Scale bars are 10 km. See Fig. 1 for locations. Anaglyph from PELR_P_LORRI_STEREO_MOSAIC and PEMV_01_P_MVIC_LORRI_CA.

The fluted terrain appears to be incised into a methane-rich mantle (Grundy et al., 2016) extending southward from the North Polar region which typically displays a rough, irregular topography north of the dissected region (i.e., the northern margin of Fig. 1). The depressions into which the flutes terminate commonly display an N_2 signature (Grundy et al., 2016).

In some locations fluted terrain transitions on overlying plains to washboard terrain discussed by Moore et al. (2016). Washboard terrain consists of parallel sets of north-south trending low ridges and troughs spaced about 1 km crest to crest, with individual ridges often exceeding 20 km in length. Examples occur on flat uplands in Figs. 9 and 10. The origin of washboard terrain is uncertain, but may be related to sublimation, aeolian, or glacial processes. Superposition relationships are uncertain except in a few locations where washboard ridges appear to be superimposed on flutes.

3.2. Dendritic valleys

Parts of the rolling, mantled terrain northeast of ***SP*** are dissected by interconnected valleys, which locally occur in a distinct dendritic pattern (Figs. 11, S4). Fig. 11(b) shows valley connections interpreted from stereo anaglyphs (e.g., Fig. S4). Given the limited resolution of the anaglyph image pairs (~0.5 km/pixel), interpretation of valley structure is partly subjective. However, the valleys are organized much as terrestrial drainage networks, with headwater valleys being relatively steep and trunk valleys with gentle slopes, with a few networks clearly reaching 3rd order. Most of the networks terminate in broad depression several tens of kilometers across but lack obvious depositional landforms extending beyond the terminus. Relief between ridge tops and the deeper valleys is typically 1.5 to 2 km. Some networks, however, appear to multiply interconnect and some clearly terminate in, or are interrupted

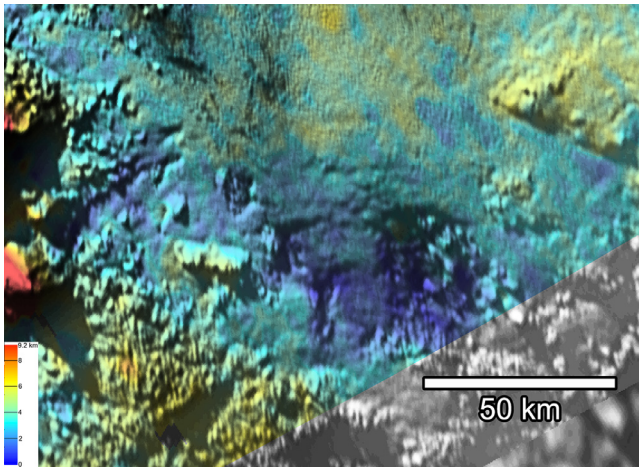

Fig. 8. Steep gradient in **SP** ices into a deep depression at the south end of **SP**. Lobate steps in ice suggest active transport into the depression. Overall N-S relief on ice surface is ~2 km. Image centered at 183.6°E, 22.1°S. See Fig. 1 for location. MVIC image base PEMV_01_P_MVIC_LORRI_CA with topography from partial stereo coverage with LORRI PELR_P_LORRI_STEREO_MOSAIC. Equirectangular projection. North is up.

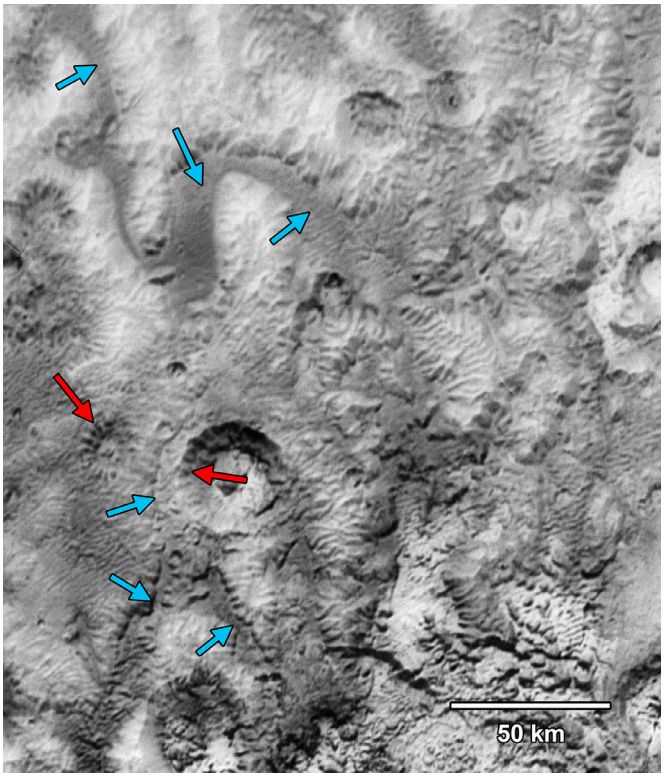

Fig. 9. Example of fluted valley morphology. Red arrows point to interior crater walls with ridge and trough erosional texturing. Troughs in fluted terrain are typically spaced 3 km apart and extend from summits of ~1.5 to 2 km high ridges downslope to end abruptly at the floor of depressions. Blue arrows point to elongated troughs. The flatter, upland areas have an overprint of washboard texture oriented NE-SW. Image centered at 154.0E, 49.4 N. MVIC 340 m/pixel PEMV_01_P_MVIC_LORRI_CA. Mercator projection. See Fig. 1 for location. North is up (For interpretation of the references to color in this figure legend, the reader is referred to the web version of this article).

by, enclosed depressions, such as apparent crater floors. The valley systems are entrenched into a broad, relatively smooth-surfaced mantle with a strong methane spectral signature with subsidiary N_2. The depressions into which the valleys debouch typically have an N_2 signature but less methane (Grundy et al., 2016).

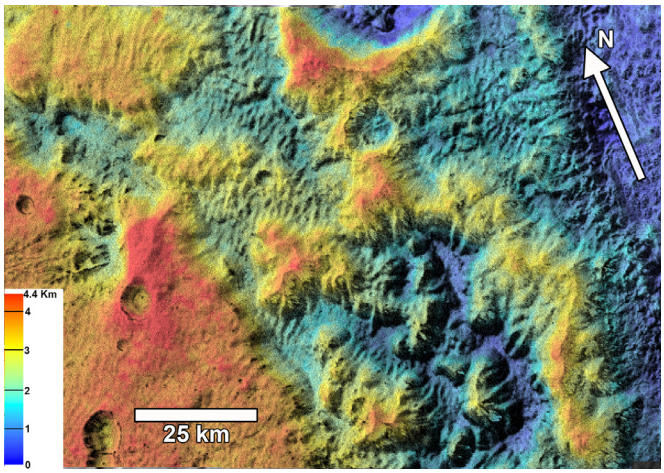

Fig. 10. Fluted terrain located to the southeast of Fig. 8. 93 m/pixel LORRI image PE:R_P_MVIC_LORRI_CA with elevation shading from stereo coverage with PELR_P_LORRI_STEREO_MOSAIC. Total relief in red to blue shading is about 4 km. Uplands at lower left has washboard texture overprint. See Fig. 1 for location. (For interpretation of the references to color in this figure legend, the reader is referred to the web version of this article).

3.3. Mountainous dissection

Somewhat intermediate between the fluted and dendritic patterns of dissection is a deeply-dissected region shown in Figs. 12, S5 which slopes steeply toward the flat surface of ***SP*** (bottom of image). The overall relief is about 2.5 km, and ridge to valley relief is typically about 1.5 km. The walls of the major ridges are dissected by ridge and trough patterning similar in scale to the fluted terrain. The major valleys are organized into crude dendritic patterns, but some terminate in blind depressions and others have irregular gradients.

3.4. Plateau dissection

A broad plateau at the center left of Fig. 13 is dissected by a series of trough-like valleys radiating from a depression (probable degraded impact crater) at the center left edge of the figure. These troughs then converge toward several broad, deep trunk valleys (red arrows), creating a crude dendritic pattern. The largest of the deep valleys in the center of the image is broadly curved and of nearly uniform width and possibly with a U-shaped cross section. The tributary valleys enter at steep gradients into the deeper troughs, and some junctions may be “hanging” above the trunk valleys.

3.5. Alpine terrain

Southwest of ***SP*** an uplands region displays a morphology characterized by dissected mountainous ridges surrounded by plains and broad valleys. Unfortunately, this region is less well characterized by New Horizons data, being imaged by lower-resolution coverage and partially being thinly mantled by dark materials, presumably tholins, which effectively reduce image resolution by lowering the image signal to noise ratio. A ~90 km long dissected ridge in Fig. 14 is capped by methane ice, providing a superficial resemblance to terrestrial ice-capped mountain chains. This mountain chain with its fluted terrain-like dissection is surrounded on its southern and western margins by 5–6 km wide, flat-floored valleys in a crude dendritic pattern (red arrows). A larger region is shown in Fig. 15. Isolated methane-capped mountain chains extend from north to south in a 100-km wide band left of center. The mountain chains are ringed by low-relief plains, into which

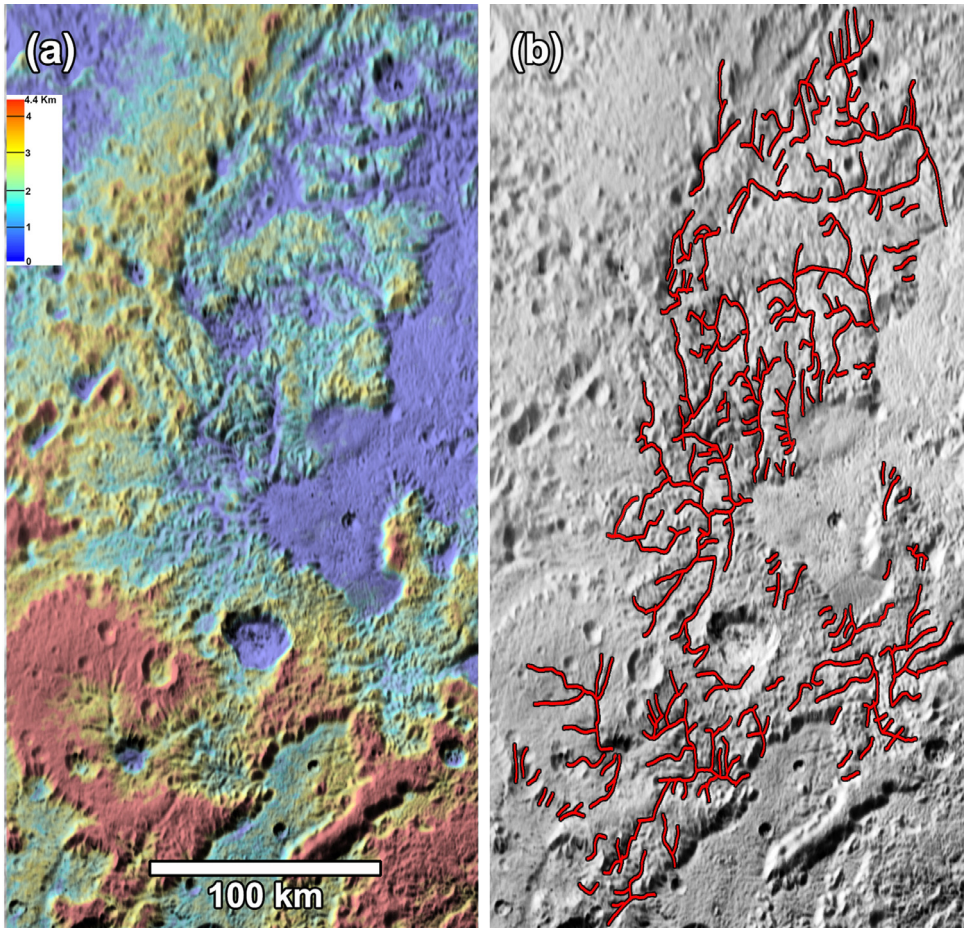

Fig. 11. Dendritic valley networks. (a) shows regional view and (b) shows interpreted valley networks. Lambert conformal projection of PEMV_01_P_MVIC_LORRI_CA 340 m/pixel image. See Fig. 1 for location. See Fig. S4 for a stereo anaglyph image of this region. North is up. Topographic relief within image is about 3.5 km.

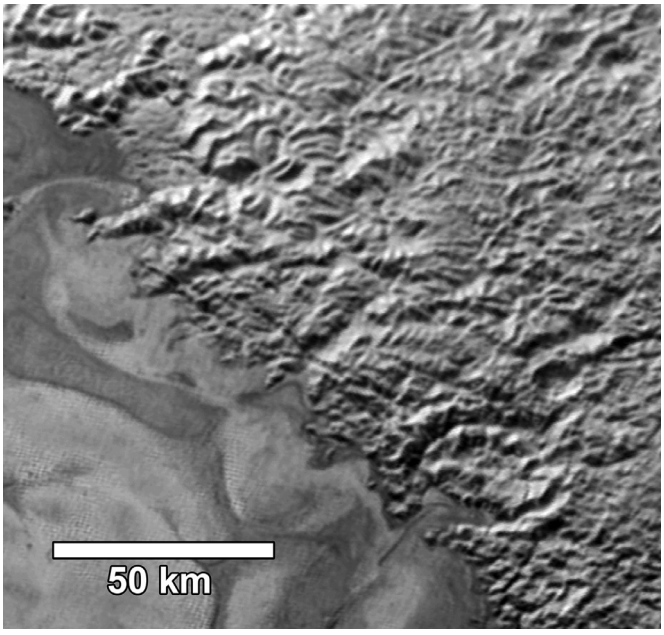

Fig 12. Mountainous style of valley dissection. Sputnik Planum ices along lower border. Image centered at about 189.9E, 46.2 N. Image from MVIC PEMV_01_MVIC_LORRI_CA at 340 m/pixel. See Fig. 1 for location. See Fig. S5 for a stereo anaglyph version of this region. North is up

are incised several valley systems which drain westward. The valley complexes numbered 4–6 are deeply incised by valleys several km wide. Valleys 1–3 are bright-floored and apparently lack deep incision. They connect to light-toned smooth plains at their western terminus. Valleys 7–9 are the plateau-style dissected valleys discussed earlier, and several other possible examples occur near the bottom right of the image.

3.6. Long valleys

A number of long linear depressions, some of which are crudely branched, are scattered on the uplands surrounding SP in areas associated with the valley features described above. These include the incised valleys shown in Figs. 9–11, 13, and the larger valleys in the Figs. 14 and 15. These and others are mapped in Fig. 16. These valleys do not have the linearity and parallel walls generally associated with structural depressions, and in the case of Fig 9 display a meandering course.

3.7. Interpretation of dissected terrains

Moore et al. (2016) discuss a range of processes that might have sculpted the dissected terrains, as summarized below:

1. Shear failure of the underlying materials via slow or rapid mass movments.
2. Accumulation and avalanching failure of ices accumulated from the atmosphere.

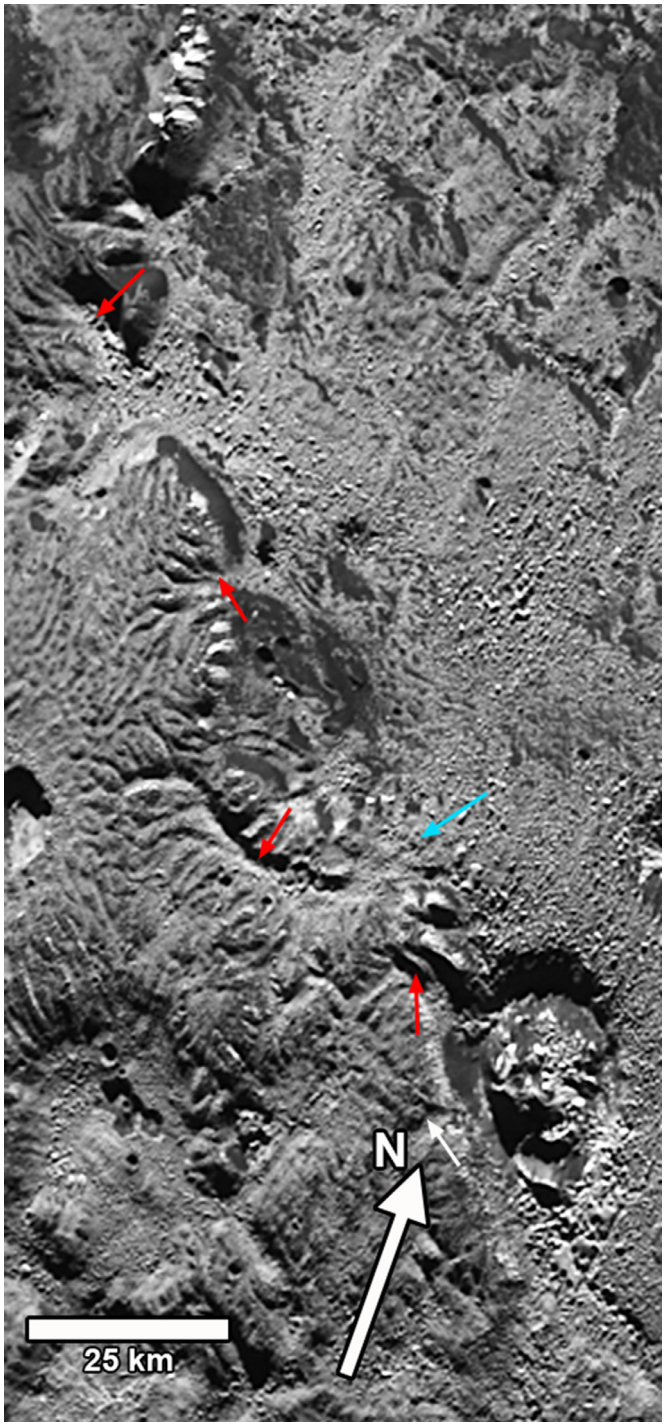

Fig. 13. Plateau style of valley dissection. Shallow trough-like valleys radiate across a sloping plateau sloping away from crater along center-left border. These valleys then converge into deeply incised troughs 2-4 km wide (red arrows) interpreted to be glacially scoured, "U"shaped valleys. Blue arrow points to a possible fan-shaped deposit at the terminus of the largest trough. Part of PEMV_01_P_MVIC_LORRI_CA image. (For interpretation of the references to color in this figure legend, the reader is referred to the web version of this article).

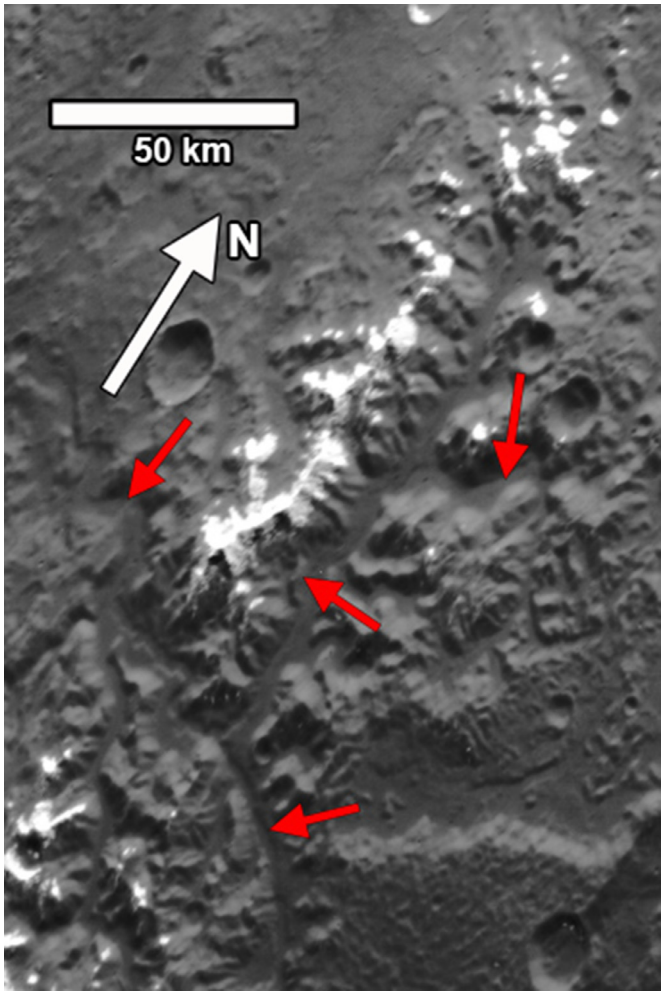

Fig. 14. Alpine style of dissection. High peaks are covered with methane frost, and remainder of image is thinly mantled with dark tholins. Note flute-like dissection of mountain slopes. Red arrows point to 4-6 km wide, flat-floored valleys. MVIC 340 m/pixel image PEMV_01)P_MVIC_LORRI_CA centered at 146.9°E, 6.5°S. See Fig. 1 for location. (For interpretation of the references to color in this figure legend, the reader is referred to the web version of this article).

3. Surface ice accumulation, glacial flow, and erosion. This is the dominant mechanism for erosion by valley glaciers on Earth (Anderson et al., 2006; MacGregor et al., 2009), where the equivalent ice on Pluto would be N_2-rich.
4. Erosion beneath thick ice sheets, such as ice streams at the margins of terrestrial plateau glaciers, such as at Greenland and Antarctica (Kessler et al., 2008).
5. Erosion by precipitation of volatiles as rain or snow, followed by erosion by liquid runoff, which accounts for most terrestrial valley networks (Howard, 1994).

Mechanisms 1 and 2 could potentially contribute to formation of the steep fluted slopes, but are unlikely to contribute to erosion of the larger dendritic valleys because of their low gradients. In addition, these mechanisms tend to deposit transported material close to their sources as fans or lobate deposits. Such depositional forms have not been identified, although they, like the glacial ice, might have been lost by sublimation. Terrestrial valley glaciers are competent agents of erosion, long-distance transport, and deposition. Most terrestrial valley glaciers occupy former fluvially-sculpted valley networks (e.g., Sternai et al., 2012); whether ice accumulating on undissected uplands would sculpt dendritic valley networks is uncertain. Most terrestrial valley glaciers are warm-based, with meltwater production that contributes to basal sliding and accompanying substrate erosion by abrasion and quarrying (e.g., Herman et al., 2011; Anderson, 2014). Cold-based ice sheets on Earth and Mars have generally been considered to be

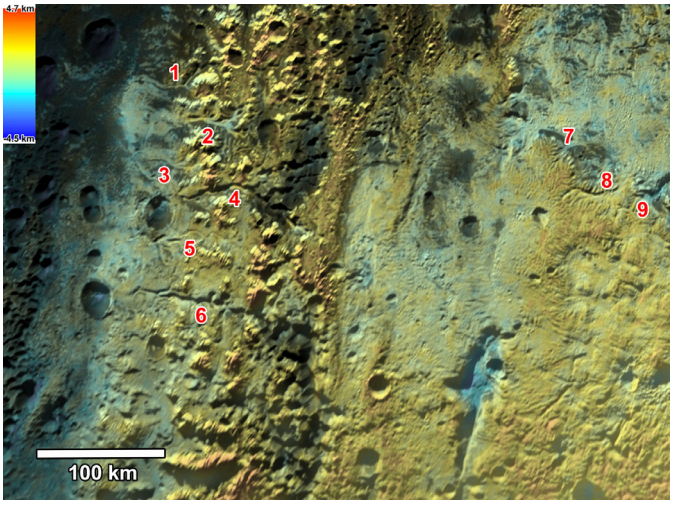

Fig. 15. Alpine glaciation with valley systems. Isolated mountain chains left of image center are capped with methane frost and are surrounded by low-relief plains. Light-toned dendritic valleys 1–3 lead downslope from alpine peaks to light-toned deposits. These valleys appear not to be deeply incised and may contain N_2 ice deposits. Deeply-dissected valleys 4–6 similarly lead from alpine mountains and plains toward the west, terminating in the cratered plains. Valleys 7–9 are plateau-style dissection shown in higher resolution in Fig. 13. MVIC 500 m/pixel image PEMV_01_P_MPAN1 centered at 147.9°E, 23.4°S. North is up.

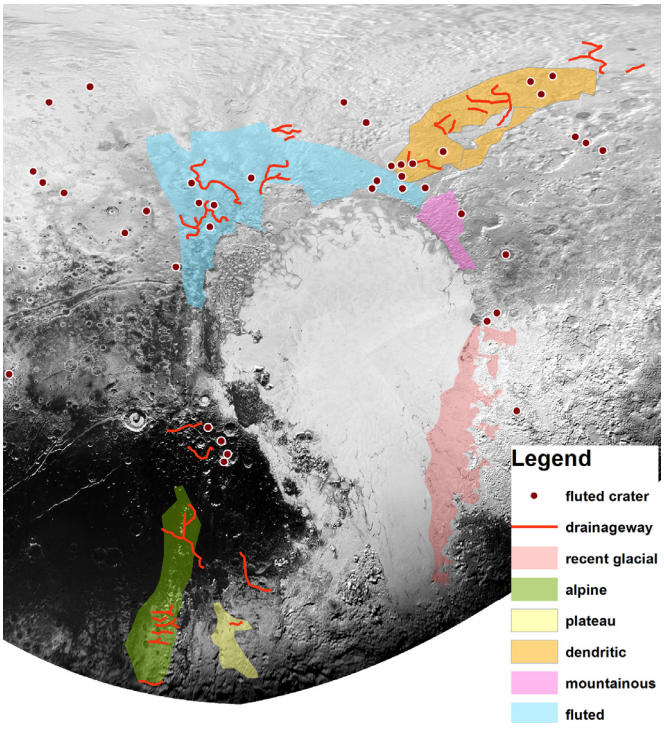

Fig. 16. Summary of terrain types discussed in paper. Red and white dots mark locations of carters whose interior walls display fluted morphology. Red "drainageway" lines are major linear depressions that are suggested to have been eroded by glacial erosion, possibly including liquid N_2 basal flow. North is up. (For interpretation of the references to color in this figure legend, the reader is referred to the web version of this article).

inefficient in eroding their beds (Head and Marchant, 2003; Gjermundsen et al., 2015). Erosion by nitrogen ice flowing over a water ice or particulate-mantled substrate on Pluto might be aided by their lower density. Thick enough accumulations of nitrogen-rich ices (~1–2 km for reasonable geothermal gradients (McKinnon et al., 2016) could result in basal melting, which can lubricate the base of the glacier and substantially increase its capacity for erosion. Stereo imaging in the dendritic valley and mountainous terrains (Figs. S4 and S5) suggests some valleys end in depressions or have irregular profiles, which is a characteristic of terrestrial valley glacier erosion (although post-formation processes may have affected the Pluto valleys). The plateau valley networks on Pluto are suggestive of some terrestrial glacial valley networks with broad, deeply incised trunk valleys and hanging tributaries.

Erosion by precipitation and runoff is impossible in Pluto's current environment, and would require a dramatically thicker past atmosphere (Strobel, 2008; Singer and Stern, 2015), although Stern et al. (2016) suggest atmospheric cycles may episodically raise surface temperatures to the point of melting N_2. Even if surface temperatures do not reach the freezing point of N_2, flow rates would be enhanced and melting would occur at shallower depth. We conclude that the most reasonable explanation for formation of Pluto's dissected terrains is glacial erosion by former accumulations of nitrogen-rich ices.

Although glaciation is suggested in large part by elimination of other possibilities, most of these landscapes lack many distinctive features of terrestrial glaciation. The landscape types most similar to terrestrial glaciation are the alpine landscapes of Figs. 14 and 15. Depositional features such as moraines and outwash plains have not been identified, possibly in part because of image resolution limitations. In general there is a fundamental discrepancy between the volume of material excavated to form the dissected landscapes and the lack of any identifiable corresponding deposits. Valleys often have large internal depressions and even large valleys have no identifiable exit path. Most troublesome to explain based upon terrestrial experience is the fluted terrain (Figs. 9 and 10) because most of the dissected troughs extend all the way to the floor of depressions without obvious corresponding deposits or evidence of longitudinal flow or appreciable erosion along the axis of the major depressions.

Glaciers composed of N_2 on Pluto, however, would have characteristics and behavior very different from water ice glaciation on Earth. One essential difference is that N_2 ice will not expand upon freezing, so that freeze-thaw fracturing will not occur. Freeze-thaw is thought to be the dominant process creating the headwall erosion producing cirques, arêtes, and horns in terrestrial mountain glaciation (Matsuoka and Sakai, 1999; Hales and Roering, 2009; Sanders et al., 2012; Mitchell and Humphries, 2015), so these features would not be expected on Pluto, although fatigue through thermal cycling has been implicated in rock weathering (Hall and André, 2001; McFadden et al., 2005). Nitrogen ice is also denser than water ice at Pluto's temperatures, so that if it were flowing over the water ice substrate on Pluto, any dislodged water ice could be floated and carried away, potentially robbing the basal N_2 flow of abrasive debris. Nitrogen ice may in fact, be a very poor agent for eroding the water ice that is assumed to form the crust of Pluto. If N_2 ice accumulated to a depth of 1–4 km (depending upon the geotherm) it might be subject to basal melting and subice drainage. Liquid N_2 is less dense than N_2 ice and be subject to surface breakout flooding if flow rates were sufficient to prevent freezing.

Most of the valley features described above appear to have been eroded into mantling deposits. These have uncertain composition. Most have a methane spectral signature, but might be composed of a wide range of materials. It is likely, however, that these deposits are porous, fine-grained, less dense than nitrogen ice, and poorly indurated – properties that suggest they should be readily eroded by flowing N_2. Because of the inverted density stratification of N_2 ice and its substrate, it is difficult to predict the detailed morphologies that would be expected from glaciation on Pluto. Such glaciation, however, appears to be the most viable explanation for the observed features.

Overall, the spatial variation in morphology of the glacial features is likely to be a response to local topographic setting, substrate properties, latitudinal variations in insolation, and variation in depths and durations of ice accumulation.

4. Inferred glacial history of Pluto

Sputnik Planum has been suggested to be the center of an ancient large impact basin, with the highlands surrounding it on three sides to be the rim complex (Schenk et al., 2015; McKinnon et al., 2016). A well-defined rim has not been identified on the southern side. The highlands comprising the rim complex to the north and west are densely cratered and likely date to the late heavy bombardment. A series of methane-rich mantles covers most of the northern latitudes. The inferred paleo-glacial landforms in the northern latitudes are largely eroded into these mantles and thus post-date them. The paleo-glacial features southwest of ***SP*** lie within and to the south of the densely-cratered Cthulhu Regio. The glacial features, however, likewise may be developed into discontinuous regional mantles. A number of fresh-appearing 5–15 km diameter craters appear to be superimposed upon the glacial landforms and the basin floors into which they appear to have drained, suggesting that this glaciation was not geologically recent (albeit superposition relationships are difficult to assess). The inferred presence of deep N_2-rich ices at the time of glacial activity suggests that the inventory of N_2 had declined over geologic time, probably by loss to space. Alternatively, there might have been a one-time, or episodic, mechanism that released large amounts of N_2 from the subsurface that was deposited on the uplands surrounding ***SP*** and was then gradually lost or recycled.

Perhaps the most spectacular feature discovered on Pluto is the discontinuous range of water-ice mountains embedded within ***SP***, including Hillary, Norgay, Bare, and al-idrisi Montes (Fig. 17). These mountains occur as disordered and probably rotated blocks of sizes ranging in size up to 40 km (Figs. 1, 17). They are separated 20–130 km from the western edge of ***SP*** by fields of smaller blocks and isolated patches of ***SP*** ices. Their origin is uncertain. Their appearance suggests that they are fragments of ice crust, perhaps fractured by the impact forming ***SP***. The simplest explanation, that they are essentially icebergs suspended in denser N_2 ices and floated to their current location, is unlikely given the small density contrast between N_2 and water ices and the many kilometers thickness of N_2 ice that would be required to support the larger blocks (Moore et al., 2016). Here we suggest a different mechanism – dislodgement from the fractured ice crust and transport by the traction forces associated with N_2 glacial flow from the surrounding highlands into ***SP***. This scenario is shown in Fig. 17, in which white arrows suggest the flow directions. The al-idrisi Montes lends support to this scenario – the whole block, if translated about 60 km to the NNW, would align with the present edge of ***SP***. Immediately to the NE of the al-idrisi Montes is a ~80 km block of the highlands bordering ***SP*** that slopes sharply toward SP and has a high scarp on its anti-***SP*** side. A topographically low region about 20 km wide separates the block from the main highlands. We suggest that this is a block that was detached, rotated, and transported a short distance toward SP by deep glacial ice covering the uplands. A prominent structural trough about 60 km across parallels the western margin of ***SP***, separating a narrow strip of highlands crust from the uplands to the west (Fig. 17). This may represent an additional partial detachment caused by flowing ice. These relationships are consistent with the origin of the mountain ranges by detachment and translation of highlands crust into ***SP***. The case for the involvement of glacial ice is, however, circumstantial. This mechanism does potentially remove the necessity for floating the large ice mountains in a deep reservoir of N_2 ice. If glaciation were the mechanism transporting the mountain blocks, the timing of this relative to the observed highlands valley features attributed to glacial erosion is uncertain, but could be much earlier.

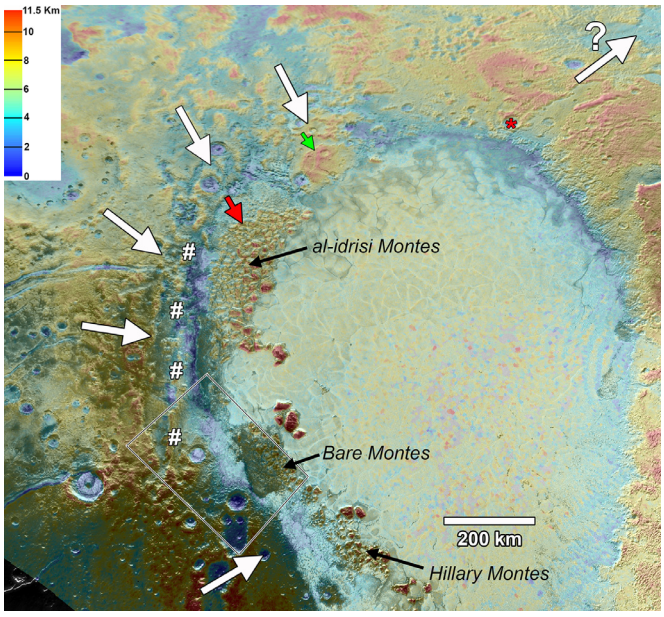

Fig. 17. Interpretation of origin of water ice mountain blocks along western boundary of **SP**. Red arrow shows how al-idrisi mountains could be translated from highlands boundary onto **SP**. White arrows show inferred direction of movement of mountain chains inferred to detach from highlands. "#" symbols show a chain of highlands separated from the main highlands to the west by a structural trough that may have been translated a shorter distance. Green arrow points to steeply-sloping block interpreted to have been tilted and separated by a few km from the highlands. The suggested cause of detachment and transport of highland crust is by flow of deep N_2 glaciers from the highlands into **SP**. The arrow on the highlands northeast of SP is aligned with linear features suggestive of sculpting by glacial flow into or out of SP. Parallel ridges extending from the crater indicated by red star suggest erosion by glacial flow out of **SP** onto the uplands eroding or depositing materials downstream from the crater rims, although this seems contrary to the inward flow suggested for the eastern boundary of **SP**. Box shows location of Fig. 18. North is up. On ***SP*** the slope toward the NW edge is real, but the apparent bowing upward of the central floor is uncertain, pending better calibration of camera pointing. (For interpretation of the references to color in this figure legend, the reader is referred to the web version of this article).

A series of dark, nearly parallel ridges occur on a plateau bordering the Bare Montes on its western edge (Fig. 18). These appear to be superimposed on underlying lighter-toned materials (water ice?). We tentatively suggest these may be recessional moraines of tholins deposited as the N_2 ice glaciers responsible for entraining and translating the ice mountains retreated.

The above scenario may, however, be contraindicated by the apparent young age of the ice mountains in ***SP***. No unambiguous craters are found, although a number of km-scale round depressions are candidates. Craters are difficult to recognize on this mountainous terrain, and might be obliterated by mass wasting. The upland glaciation discussed earlier appears to be significantly older, given possible superimposed craters. The lack of obvious ejecta sheets and possible subsequent modification, however, complicates assessment of age relationships.

5. Conclusions

Active N_2 ice glaciation occurs along the eastern boundary of ***SP***, funneling ice from upland plateaus onto ***SP*** through 2-5 km troughs. This is supported by morphological evidence (topographic relationships, flow lines converging to troughs and spreading downstream onto ***SP***), spectral evidence of a dominant N_2 composition, as well as experimental data indicating sufficiently low viscosity of N_2 ice at Pluto's surface temperatures. A glacial ice

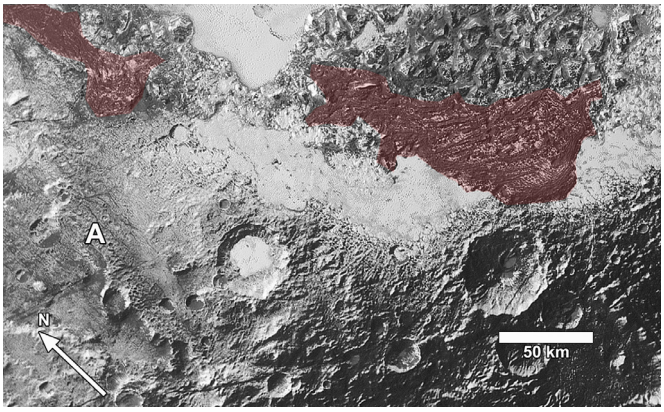

Fig. 18. Mountainous blocks and densely cratered uplands on western boundary of **SP**. The red-shaded regions of dark bands appear to be superimposed on a plateau of water ice blocky mountains, and are tentatively interpreted as recessional moraines of tholin-rich materials deposited during retreat of glaciers formerly covering the region. Note tilted crustal block at "A". Part of LORRI PELR_P_LEISA_HIRES mosaic at 260 m/pixel. See Fig. S6 for a stereo anaglyph version of this region. (For interpretation of the references to color in this figure legend, the reader is referred to the web version of this article).

cycle may be involved, with N_2 ice sublimated from ***SP*** being redeposited on the uplands and returned to ***SP*** as glacial flow. The long-term evolution of this glaciation is uncertain.

The uplands to the west, north and northeast of SP have been dissected by linear depressions (valleys) of diverse but intergrading morphologies, here characterized as fluted, dendritic, mountainous, plateau, and alpine. A variety of possible formative processes have been evaluated here and in Moore et al. (2016), with a favored interpretation as features carved by past glaciation. Depositional glacial features such as moraines, eskers, and outwash have not been unambiguously identified. N_2 glaciation would differ in important respects from terrestrial ice glaciation, particularly in the absence of freeze-thaw weathering of adjacent topography and the higher density of N_2 ice relative to probable substrates (porous ice and mantling deposits). If N_2 glacial ices were sufficiently thick (1 to a few km) they may have experienced basal melting. The age and history of the paleo-glaciation is uncertain.

We hypothesize that N_2 paleo-glacial flows may have detached water ice bedrock blocks with length scales of tens of km from the uplands surrounding SP and transported them up to 130 km into ***SP***, forming the prominent mountain ranges of jumbled ice blocks.

Acknowledgments

Support for the authors was made possible through NASA's *New Horizons* mission within the New Frontiers program.

Supplementary materials

Supplementary material associated with this article can be found, in the online version, at doi:10.1016/j.icarus.2016.07.006.

References

Anderson, R.S., 2014. Evolution of lumpy glacial landscapes. Geology 42 (8), 679–682.
Anderson, R.S., Dünforth, M., Colgan, W., et al., 2012. Far-flung moraines: Exploring the feedback of glacial erosion on the evolution of glacier length. Geomorphology 179, 269–285 doi:210.1016/j.geomorph.2012.1008.1018.
Anderson, R.S., Molnar, P., Kessler, M.A., 2006. Features of glacial valley profiles simply explained. J. Geophys. Res. 111 (F01004). doi:10.1028/2005JF000344.
Archinal, B.A., A'Hearn, M.F., Conrad, A., et al., 2011a. Celest. Mech. Dyn. Astron. 110, 401.
Archinal, B.A., A'Hearn, M.F>, Bowell, E., et al., 2011b. Celest. Mech. Dyn. Astron. 109, 101.
Binzel, R.P., Earle, A.M., Young, L.A., et al. New Horizons Geology and Geophysics Imaging Team, 2016. Climate zones on Pluto and Charon. Icarus (this issue).
Durham, W.B., Stern, L.A., 2001. Rheological properties of water ice – Applications to satellites of the outer planets. Annu.Rev. Earth Planet. Sci. 29, 295–330.
Earle, A.M., Binzel, R.P., 2015. Pluto's insolation history: Latitudinal variation and effects on atmospheric pressure. Icarus 250, 405–412.
Earle, A.M., Binzel, R.P., Young, E.F., et al., 2016. Long-term surface temperature modeling of Pluto. Icarus (this issue).
Eluszkiewicz, J., Stevenson, D.J., 1990. Rheology of solid methane and nitrogen: Applications to Triton. Geophys. Res. Lett. 17 (10), 1753–1756.
Fracassi, P.F., Cardini, G., O'shea, S., et al., 1986. Solid and liquid carbon monoxide studied with the use of constant-pressure molecular dynamics. Phys. Rev. B 33, 3441–3447 3410.1103/PhysRevB.3433.3441.
Fukushima, E., Gibson, A.A.V., Scott, T.A., 1977. Pressure dependence of the melting and α-β phase transition temperatures of carbon monoxide. J. Low Temp. Phys. 28 (1/2), 157–165.
Gladstone, G.R., Stern, S.A., Ennico, K., et al., and the New Horizons Science Team, 2016, The atmosphere of Pluto as observed by New Horizons, Science, 351(6279), 1280, doi:10.11.26/science.aad8866.
Gjermundsen, E.F., Briner, J.P., Akçar, N., et al., 2015. Minimal erosion of Arctic alpine topography during late Quaternary glaciation. Nat. Geosci. 8 (789-793).
Goldsby, D.L., Kohlstedt, D.L., 2001. Superplastic deformation of ice: Experimental obervations. J. Geophys. Res. 106 (B6), 11017–011030.
Grundy, W.M., Binzel, R.P., Buratti, B.J., et al., 2016. Surface compositions across Pluto and Charon. Science 351 (6279), 1283. doi:10.1126/science.aad9189.
Hales, T.C., Roering, J.J., 2009. A frost "buzzsaw" mechanism for erosion of the eastern Southern Alps, New Zealand. Geomorphology 107 (3-4), 241–253.
Hall, K., André, M.-F., 2001. New insights into rock weathering from high-frequency rock temperature data: An Antarctic study of weathering by thermal stresses. Geomorphology 41, 23–35.
Hansen, C.J., Paige, D.A., Young, L.A., 2016. Pluto's climate modeled with new observational constraints. Icarus 246, 183–191 doi:110.1015/j.icarus.2014.1003.1014.
Head, J.W., Marchant, D.R., 2003. Cold-based mountain glaciers on Mars: Western Arsia Mons. Geology 31 (7), 641–644.
Herman, F., Beaud, F., Champagnac, J.-D., et al., 2011. Glacial hydrology and erosion patterns: A mechanism for carving glacial valleys. Earth Planet. Sci. Lett. 310, 498–508.
Howard, A.D., 1994. A detachment-limited model of drainage-basin evolution. Water Resour. Res. 30 (7), 2261–2285.
Kessler, M.A., Anderson, R.S., Briner, J.P., 2008. Fjord insertion into continental margins driven by topographic steering of ice. Nat. Geosci. 1, 365–369.
Lellouch, E., Laureijs, R., Schmitt, B., et al., 2000. Pluto's non-isothermal surface. Icarus 147, 220–250 doi:210.1016/icar.2000.6441.
Lellouch, E., Stansberry, J.A., Emery, J.P., et al., 2011. Thermal properties of Pluto's and Charon's surfaces from *Spitzer* observations. Icarus 215, 701–716.
Leyrat, C., Lorenz, R.D., Le Gall, A., 2016. Proping Pluto's underworld: Ice temperatures from microwave radiometry decoupled from surface conditions. Icarus 260, 50–55 doi:10.1016/j.icarus.2015.1012.1016.
MacGregor, K.R., Anderson, R.S., Waddington, E.D., 2009. Numerical modeling of glacial erosion and headwall processes in alpine valleys. Geomorphology 103, 190–204.
Matsuoka, N., Sakai, H., 1999. Rockfall activity from an alpine cliff during thawing periods. Geomorphology 28, 309–328.
McFadden, L.D., Eppes, M.C., Gillespie, A.R., et al., 2005. Physical weathering in arid landscapes due to diurnal variation in the direction of solar heating. Geol. Soc. Am. Bull. 117 (1), 161–163.
McKinnon, W.B., Nimmo, F., Wong, T., et al. the New Horizons Geology, Geophysics and Imaging Theme Team, 2016. Convection in a volatile nitrogen-ice-rich layer drive Ploto's geological vigour. Nature 534, 82–87. doi:10.1038/nature18289.
Mitchell, S.G., Humphries, E.E., 2015. Glacial cirques and the relationship between equilibrium line altitudes and mountain range height. Geology 43 (1), 35–38.
Moore, J.,M., McKinnon, W.B., Spencer, J.R., et al., 2016. The geology of Pluto and Charon through the eyes of New Horizons. Science 351, 1284–1293. doi:10.1126/science.aad7055.
Paterson, W.S.B., 1994. The Physics of Glaciers. Pergamon, Trowbridge.
Petrenko, V.F., Whitworth, R.W., 1999. Physics of Ice. Oxford University Press, Oxford.
Philippe, S., Schmitt, B., Grundy, W.M., et al., 2016. CH_4-rich ices distribution at the surface of Pluto evidenced by New Horizons. In: Proceedings of Lunar and Planetary Science Conference Abstract 2757.
Sanders, J.W., Cuffey, K.M., Moore, J.R., et al., 2012. Periglacial weahering and headwall erosion in cirque glacier bergschrunds. Geology 40, 779–782 710.1130/G33330.33331.
Satorre, M.Á., Domingo, M., Millán, C., et al., 2008. Density of CH_4, N_2, and CO_2 ices at different temperatures of deposition. Planet. Space Sci. 56, 1748–1752.
Schenk, P.M., McKinnon, W., Moore, J.,M., et al., 2015. A Large Impact Origin for Sputnik Planum and Surrounding Terrains, Pluto?. American Astronomical Society Division of Planetary Sciences Meeting #47, id.200.06.
Schmitt, B., Philippe, S., Grundy, W.M., et al., 2016. Mixing and physical state of Pluto's surface materials from New Horizons. In: Proceedings of Lunar and Planetary Science Conference Abstract 2794.
Scott, T.A., 1966. Solid and liquid nitrogen. Phys. Rep. 27 (3), 89–157.
Singer, K.N., Stern, S.A., 2015. On the provenance of Pluto's nitrogen (N_2). Astrophys. J. Lett. 808:L50 (5 pp), doi:10.1088/2041-8205/808/2/L50.

Stern, S.A., Bagenal, F., Ennico, K., et al., 2015a. The Pluto system: Initial results from its exploration by New Horizons. Science 350 (292), 291–298.
Stern, S.A., Binzel, R.P., Earle, A.M., et al. New Horizons Science Team, 2016. Past epochs of significantly higher pressure atmospheres on Pluto. Icarus (this issue).
Stern, S.A., Porter, S., Zangari, A., 2015b. On the roles of escape erosion and the viscous relaxation of craters on Pluto. Icarus 250, 287–293 doi:210.1016/j.icarus.2014.1012,1006.
Sternai, P., Herman, F., Champagnac, J.-D., et al., 2012. Pre-glacial topography of tahe European Alps. Geology 40 (12), 1067–1070.
Strobel, D.F., 2008. N_2 escape rates from Pluto's atmosphere. Icarus 2008, 612–619.
Trowbridge, A.J., Melosh, H.J., Steckloff, J.K, et al., 2016. Vigorous convection as the explanation for Pluto's polygonal terrain. Nature 534, 79–81. doi:10.1038/nature18016.
Umurhan, O.M., Howard, A.D., Moore, J.M., et al., 2016. Modeling glacial flow on and onto Pluto's Sputnik Planum. Icarus (this issue).
Yamashita, Y., Kato, M., Arakawa, M., 2010. Experimental study on the rheological properties of polycrystalline solid nitrogen and methane: Implications for tectonic processes on Triton. Icarus 207, 972–977 doi:910.1016/j.icarus.2009.1011.1032.